

AirLine: Efficient Learnable Line Detection with Local Edge Voting

Xiao Lin¹ and Chen Wang²

Abstract—Line detection is widely used in many robotic tasks such as scene recognition, 3D reconstruction, and simultaneous localization and mapping (SLAM). Compared to points, lines can provide both low-level and high-level geometrical information for downstream tasks. In this paper, we propose a novel edge-based line detection algorithm, AirLine, which can be applied to various tasks. In contrast to existing learnable endpoint-based methods which are sensitive to the geometrical condition of environments, AirLine can extract line segments directly from edges, resulting in a better generalization ability for unseen environments. Also to balance efficiency and accuracy, we introduce a region-grow algorithm and local edge voting scheme for line parameterization. To the best of our knowledge, AirLine is one of the first learnable edge-based line detection methods. Our extensive experiments show that it retains state-of-the-art-level precision yet with a 3–80× runtime acceleration compared to other learning-based methods, which is critical for low-power robots.

I. INTRODUCTION

With the growing need for autonomous robots in recent years, algorithms enabling robots to sense and interpret the real world through vision are becoming increasingly popular and demanded. Tasks like scene recognition [1] and simultaneous localization and mapping (SLAM) [2] are crucial for many applications such as autonomous driving [3] and reconstruction [4]. To achieve matching and mapping in images from different views of the same scene, the prevailing solutions are often based on interest points [5], [6] with descriptors, or descriptive lines [7], [8]. A powerful point or line detector can provide a more consistent and informative result, significantly boosting the accuracy of image matching [9], camera localization [10], and environment mapping [11].

Despite the promising progress, the performance of line detection is still unsatisfactory for real-time robotic tasks. On the one hand, traditional hand-crafted methods like LSD [12] and Hough Transform [13] with canny edge detection [14] are efficient but sensitive to illumination and heavily rely on manual parameter tuning, often yielding unstable results and lacking generalization ability. They are computationally cheap but not adaptive or learnable, which might result in inconsistent detection in varying environments. Some recent methods like [15] outperform LSD but they still have a limited perceptual ability and lack adaptivity.

On the other hand, learning-based line detection methods are relatively robust but often computationally expensive [16]. For example, LCNN [17] detects line junctions and

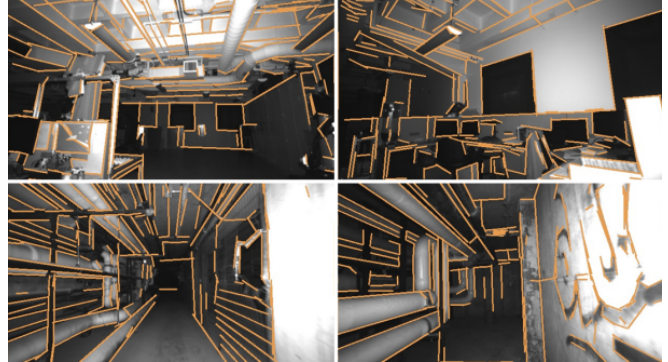


Fig. 1: AirLine is a lightweight line segment detector designed for robotic tasks. It succeeded in detecting most structural lines and be robust to viewport change and texture noise as the camera move from scene to scene.

then learns to connect lines from points. Though the accuracy is appreciable, the inference is extremely slow. The state-of-the-art model LETR [18] achieves higher speed, but it is still not efficient enough to run in real time. Another learning-based approach is [19], which performs infinitely-long semantic line detection with Hough Transform and deep-learned models. However, it is not suitable for line segment detection since Hough transform can only detect infinitely long lines and introduces potential errors by the limited discrete parametric space.

One interesting phenomenon we observed is that most existing learnable line detection methods like LCNN are endpoint-based methods, which are sensitive to geometrical conditions of the environments since not all lines contain significant endpoints, or that a large number of endpoints may exist in the environment, which can increase computation drastically. To solve this problem, we introduce a learnable edge-based line detection method, AirLine, which can extract line segments directly from edges, resulting in better generalization and stability. Additionally, to retain the advantage of the speed of classical methods and the perceptual ability of learning-based methods, we propose a novel local edge voting scheme with a conditional region-growing strategy for precise end-point localization. This makes AirLine much faster than other learning-based methods and more robust and accurate than classical methods.

In summary, the main contributions of this paper are:

- We propose AirLine, a fast, robust, and accurate edge-based line detection pipeline without explicit end-points detection, where each module is plug-and-play and can be easily substituted by other better methods.

¹Xiao Lin is with the College of Computing, Georgia Institute of Technology, Atlanta, GA 30332, USA xlin330@gatech.edu

²Chen Wang is with the Spatial AI & Robotics Lab at The Department of Computer Science and Engineering, State University of New York at Buffalo, NY 14260, USA. chenwang@dr.com

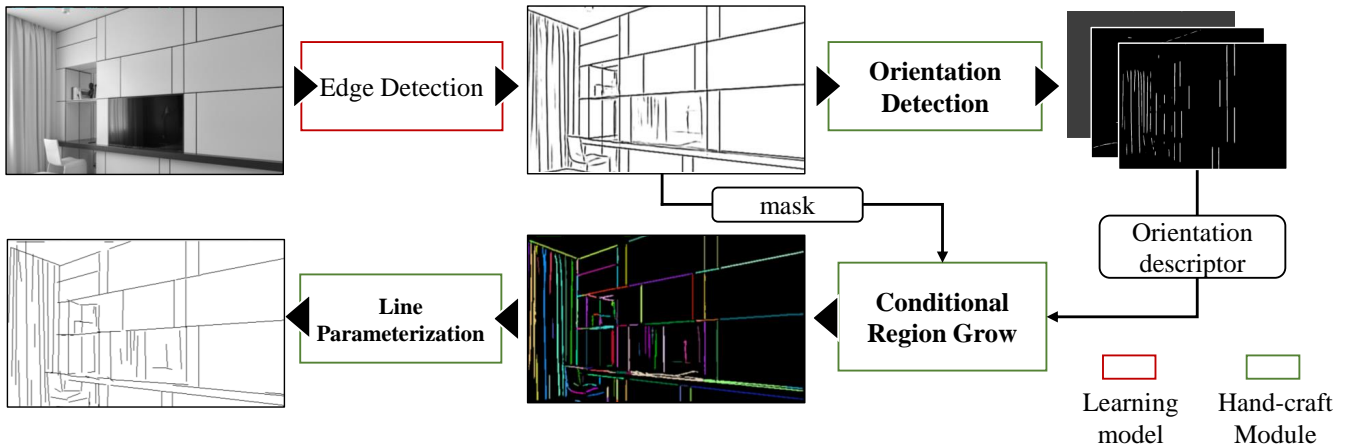


Fig. 2: The architecture of AirLine, which is extremely simple and only consists of four modules including edge detection, orientation detection, conditional region grow, and line parameterization.

- We design a new edge-to-line conversion scheme with local edge voting, which avoids the sensitivity and low efficiency of point-to-line methods, as well as the line overlapping problem and low quality of the traditional edge-to-line methods based on Hough Transform.
- We propose a new line segment detection metric based on pixel-level evaluation emphasizing edge-line consistency. We also demonstrate that AirLine retains state-of-the-art-level precision yet with a $3 - 80\times$ runtime acceleration. To the best of our knowledge, AirLine is the first learnable edge-based line detection method. The source code is released at <https://github.com/sair-lab/AirLine> to benefit the community.

II. RELATED WORK

A. Hand-crafted Algorithms

Line segment detector (LSD) [12], a classic hand-crafted line detector, remains the first preference for most line detection tasks in the robotics field. It relies on a region-growing strategy and runs extremely fast even without GPU to achieve real-time detection. In LSD, pixels with similar image gradients are grouped together to form a region and then converted to line segments by an approximated rectangle. As a step forward, Cho *et al.* [20] not only utilized gradient but also other information such as brightness and gradient intensity to further improve the performance. Some other variants like PLSD [15] developed line merging strategies but sometimes tend to over-segment. An obvious limitation of the hand-crafted approaches is that the detection is based on low-level information like image gradient and brightness, leading to the unawareness of higher-level semantic information.

B. Learning-based Algorithms

A classic learning-based algorithm is LCNN [17], which detects endpoints and learns to connect them and form line segments, making no use of edges and relying heavily on endpoint detection. The learned network pairs the detected endpoints to form line segments when the score exceeds a

certain threshold. LCNN has achieved high-quality line segment detection on widely-used datasets such as Wireframe [21] and YorkUrban [22]. However, if a large number of endpoints exist, the inference time increases significantly, making stable real-time detection not possible. HAWP [23] optimizes efficiency based on LCNN, achieving similar results in less time, but is still too computationally expensive to support real-time detection. Unlike previous methods, LETR [18] detects lines as entities and represents them similar to the diagonal line of a bounding box produced by a vectorized line segment predictor, converted from the box predictor in DETR [24]. This method has achieved state-of-the-art results on the Wireframe dataset under certain metrics, enabled end-to-end training of line segment detection, and reduced runtime variance compared to previous methods.

C. Hybrid Algorithms

Zhao *et al.* [19] proposed a hybrid pipeline to achieve semantic line detection with Hough Transform. By voting edge-like information, a line is determined by the highest-voted angle and position. A differentiable Hough Transform is used to make the pipeline learnable. Although Hough Transform works well for a few straight lines, it offers a view too global for dense line segment detection. There are also learnable versions of LSD like LSDNet [25] improving LSD by introducing learned line heat maps and orientation maps, but the learning orientation predictor is not precise and easy to train. To solve the problems above, AirLine achieves stabler short-line detection by limiting the voting region to parts of continuous edge and accurate orientation detection using hand-crafted orientation detectors on sole edges.

III. METHODOLOGY

As shown in Fig. 2, AirLine is a learnable edge-based line detection architecture that is composed of four modules including edge detection, orientation detection, conditional region-grow, and line parameterization. We next present their motivation and detailed process, respectively.

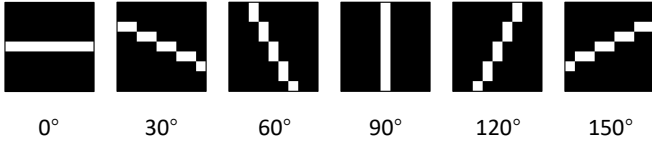


Fig. 3: The voting convolution kernels in the orientation detection module. Each channel is with a 1-pixel-wide line of a specific orientation.

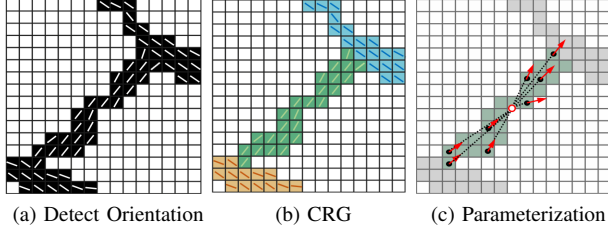


Fig. 4: A hand-craft illustration of how the orientation detection and conditional region grow help convert edges to lines. Figure (a) is an orientation map detected on the thresholded edge; Figure (b) is the result of the conditional region grow based on detected orientation; Figure (c) demonstrates the process of line parameterization: the white-red dot denotes the center m' of the region and red arrows denote the tangent vectors \mathbf{v} from each pixel in the region to m' .

A. Edge Detection

The edge detection module is used to identify potential edges making up line segments. To this end, we employ an image-to-image network to predict edges as binary images. This module plays a significant role in determining the quality of lines, as it plays a role to filter out noisy textures and ensures the continuity of edges. In our experiments, we found that the detected edges do not need to be strictly straight as long as they are distinguishable and continuous, because our proposed conditional region-grow strategy presented in Section III-C is able to detect any straight, continuous edges.

Specifically, we adopt the U-Net [26] as our edge detector. To improve the continuity of the detected edges, we impose a weak penalty on the false positive predictions with a weighted masked binary cross entropy (BCE) loss L_{edge} :

$$L_{\text{edge}} = ((1 - w) + w \cdot \tau_r(\mathbb{I}_{\mathbf{Y}=1})) \text{BCE}(\mathbf{X}, \mathbf{Y}), \quad (1)$$

where w is a weight for mask, \mathbf{X} is a prediction, \mathbf{Y} is ground truth, τ_r is a dilation operator with radius r , and $\mathbb{I}_{\mathbf{Y}=1}$ is a mask where its value is 1 if the corresponding position of \mathbf{Y} is also 1, otherwise 0. This loss function can yield stabler line detection and the method gains an appreciable generalization ability on images out of the training distribution.

B. Orientation Detection

After performing edge detection, we design an orientation detection module to predict the slope of the edges. The orientation detector is simply a convolution layer with N hand-crafted kernels for each channel. Specifically, the n^{th} channel of the kernel contains a 1-pixel-wide line with a

Algorithm 1: Conditional Region-grow (CRG)

```

 $G_X \leftarrow \phi$ 
foreach unused edge pixel  $p$  in  $\mathbf{X}$  do
   $R \leftarrow \phi$ 
   $F \leftarrow \phi$ 
   $D_R^{\text{avg}} \leftarrow D_p$ 
  add  $\eta(p)$  to  $F$ 
  while  $F \neq \phi$  do
    foreach unused pixel  $p'$  in  $F$  do
       $S \leftarrow D_{p'} \cdot D_R^{\text{avg}}$ 
      if  $S \geq T$  then
        mark  $p'$  as used
        update  $D_R^{\text{avg}}$  with  $D_{p'}$ 
        add  $p'$  to  $R$ 
        add  $\eta(p')$  to  $F$ 
    if  $|R| > m$  then
      add  $R$  to  $G_X$ 
return  $G_X$ 

```

value of 1 at an angle of $n \times \frac{180^\circ}{N}$ ($n = 0, \dots, N-1$), with the other pixels set to 0, as shown in Fig. 3. By applying the orientation detection to the edges and then performing an L_2 normalization (2), we can easily generate a N -channel orientation descriptor D_x , of which each channel describes the probability of the pixel belongs to a particular orientation.

$$D_x = \phi(\text{Conv}(\mathbf{X}, \mathbf{k})), \quad (2)$$

where D_x is the output descriptor map, ϕ is an L_2 normalization function, Conv is a convolution, and \mathbf{k} is the handcraft N -channel kernel. The convolution is applied to the thresholded edge map and generates an orientation descriptor map as visualized in Fig. 4a.

Initially, we attempted to directly predict the edge orientation map with learnable models such as U-Net, but it proved to be difficult to train and of poor precision. The advantage of employing this handcraft convolution is that we can precisely compute orientation extremely fast in parallel, especially with libraries such as PyTorch [27]. The kernels' size and number can be adjusted according to the different applications. Larger kernel sizes and more kernels might result in excessive sensitivity. In the experiments, we found that $N = 6$ provides the best overall performance in terms of accuracy, generalization ability, and efficiency.

C. Conditional Region-grow

We next introduce a conditional region-grow (CRG) algorithm to group continuous straight edges and output edge groups which will be used for line parameterization. In Algorithm 1, we first define $\eta(p)$ as an operator that returns 8 adjacent pixels around the pixel p . Then we declare F as a list to store the frontier pixels during searching, and a threshold m to skip regions with too few pixels.

Different from the region-grow algorithm in LSD, which grows the region by image gradients, we grow each region

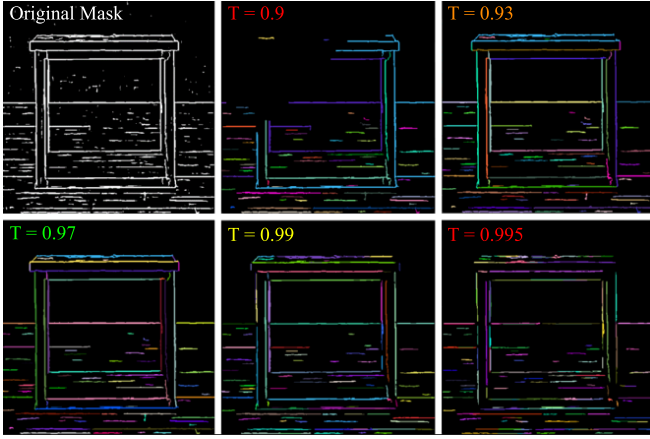


Fig. 5: This figure gives a straightforward showcase of how similarity threshold T in Algorithm 1 affects the result edge segmentation. A high T means that the conditional region-grow is sensitive to descriptor change. In this example input, $T = 0.97$ turns out to be the best threshold to keep the continuity of edges and tend not to be overgrown at corners.

along edge pixels with similar orientation descriptors produced by orientation detection to identify groups of straight edges as visualized in Fig. 4b. As a result, our algorithm can stop growing edges at turning corners. The criterion C_p of whether a pixel p will be merged into a region R can be represented as the following expressions:

$$C_p = \begin{cases} \text{True} & S_p \geq T, \\ \text{False} & S_p < T, \end{cases} \quad (3)$$

$$S_p = D_p \cdot D_R^{\text{avg}}, \quad (4)$$

where S_p describes the similarity of descriptor for pixel p and averaged grown region descriptor D_R^{avg} and T is a user-defined similarity threshold. If C_p is true, the pixel p will be grown as part of a region R and then the averaged region descriptor D_R^{avg} is updated with D_p . The threshold T is subject to change for a suitable sensitivity to orientation changes as demonstrated in Fig. 5, which can be used for edge-to-curve detection as well.

D. Line Parameterization

The final step of AirLine is to parameterize the grown straight edge groups into line segments by local edge voting. Specifically, we aim to extract the centers, tangent vectors, and endpoints for all potential lines. Though it is possible to directly calculate the tangent vectors with the regional mean orientation descriptor D_R^{avg} , in the experiments we found that parameterizing with exact pixel coordinates is more precise.

We next show how to parameterize a line with all grown pixels in a group G . In contrast to the traditional Hough transform, which uses all edge pixels across the image to vote for all lines simultaneously, we instead convert group-wise edges into lines, which can avoid interference between different groups. In detail, we first determine the center of mass \mathbf{m} as an anchor point on the line; Then vote a tangent

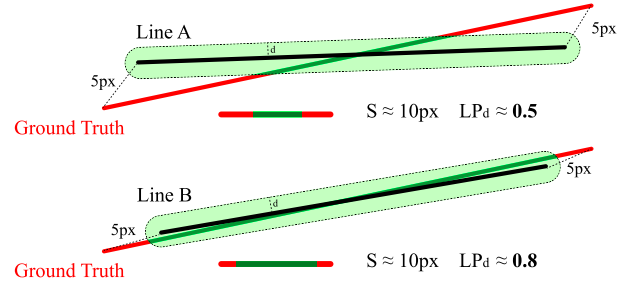


Fig. 6: Endpoint-based metric cannot well evaluate the two detected lines which has the same endpoint shifts S , while pixel-level precision is a better indicator for line detection.

vector $\hat{\mathbf{v}}$ to express the orientation of the line; Finally, the endpoints are obtained from the farthest pixel to the center. Therefore, for each line, the parameters can be calculated as:

$$\mathbf{m} = (\bar{x}, \bar{y}), \quad (x, y) \in R \quad (5a)$$

$$\hat{\mathbf{v}} = \phi \left(\sum_{(x_i, y_i) \in R} x_i - \mathbf{m}_x, \sum_{(x_i, y_i) \in R} y_i - \mathbf{m}_y \right), \quad (5b)$$

$$\mathbf{p} = \pm (\hat{\mathbf{v}} \cdot \mathbf{v}_{\max}) \hat{\mathbf{v}} + \mathbf{m}, \quad (5c)$$

where x and y are coordinates of the grown edges, $\bar{\cdot}$ indicates the average operation, ϕ is an L_2 normalization function, $\hat{\mathbf{v}}$ is the voted tangent vector, \mathbf{v}_{\max} is the longest vector from center to pixels, and \mathbf{p} are endpoints of the line, which is the final output. Fig. 4c illustrates a visualization reference for this step. At this point, the line segments have been successfully extracted using the aforementioned modules.

E. Evaluation Metric

Prior line segment detection methods, e.g., [17], [18] have typically been evaluated using the endpoint precision sAP , which defines a criterion for true positive detection:

$$\min_{(p_n, p_m) \in L} (\| \bar{p}_1 - p_n \|_2^2 + \| \bar{p}_2 - p_m \|_2^2) \leq E, \quad (6)$$

where \bar{p}_1 and \bar{p}_2 are the ground truth endpoints, p_n and p_m are detected endpoints of lines L , and E is a user-defined threshold. However, it is not reasonable for many downstream applications due to three reasons:

- 1) It disregards measurements like line length and orientation, which is crucial for many downstream tasks such as pose estimation. In many cases, long lines weigh much more than short ones in terms of semantic significance as well as geometrical information. However, as shown in Fig. 6, a line with a relatively large angle error could have a similar endpoint error as a line with the correct orientation, therefore the endpoint precision cannot faithfully reflect the effectiveness of line detection.

- 2) Some hand-crafted datasets like Wireframe [21] and YorkUrban [22] label lines in an inconsistent way, i.e., some lines are labeled in one image while similar lines are ignored in others. This indicates that line detection is a subjective task and annotators have a different definition for

TABLE I: Overall performance comparison.

Method	LP ₀	LP ₁	LP ₂	LP ₃	LP ₅	LP ₁₀	FPS
AirLine	<u>18.22</u>	<u>49.99</u>	<u>65.63</u>	<u>75.5</u>	84.21	94.52	<u>24.3</u>
LCNN	21.35	53.09	66.54	75.73	<u>83.98</u>	<u>94.03</u>	0.9
LETR	15.07	41.37	57.85	69.32	78.86	90.96	4.5
LSD	12.79	39.13	49.4	55.38	61.4	70.79	34.5

line significance. Therefore, we argue that there should be a grace tolerance to “false positive” line detection to mitigate the effects of the subjective factors.

3) A relatively low score on endpoint precision does not necessarily indicate poor performance. For example, LSD is one of the most popular line detectors, but it has an extremely low endpoint precision because it tends to detect separated segments, though the detected shorter lines are accurate.

Thus, we concluded that pixel-level line coverage precision could better reflect the quality of line detection. To solve the above problems and provide a useful perspective in the line detection task, we propose a new metric, e.g., Line Precision (LP_r) in (7), considering all reasonable lines.

$$LP_r = \frac{\sum \tau_r(\mathbf{X}) \otimes \mathbf{Y}}{\sum \mathbf{Y}}, \quad (7)$$

where τ_r denotes an dilation function with a tolerance radius r and \otimes is an element-wise multiplication operation. LP_r is designed for calculating the percentage of ground truth pixels covered by the prediction within an error range. We include Fig. 6 for a simple and straightforward interpretation. Again, we designed the metric to evaluate true positives to fairly compare both learned methods and handcrafted methods that behave differently, as a lot of “false positives” are reasonable but not labeled in the dataset. Take line B in Fig. 6 as an example, LP_d is given by dividing the area of ground truth by its intersection with the expanded output area. The two examples have similar sAP scores given the same amount of endpoint offsets, however, line B is a result better than line A in terms of orientation and position.

IV. EXPERIMENTS

A. Implementation Details

To train the U-Net edge detector, we used the masked BCE loss (1) with weight $w = 0.8$ and implemented the dilation function τ_r in the loss function using a transposed circle convolution with radius $r = 5$. An Adam optimizer [28] with an initial learning rate 5×10^{-4} (reduced by multiplying 0.3 when reaching a milestone) is used for optimization.

To make the edge detector equally sensitive to all orientations, we implemented data augmentation techniques including random rotation and brightness changes.

To create our hand-crafted orientation detector, we employed an unbiased PyTorch [27] Conv2d layer with kernels generated by OpenCV [29]. We ran the edge and orientation detector on the GPU and CRG and line parameterization on the CPU. The final output is a list of endpoints. We set the similarity threshold T to 0.98 and a minimum of pixels m for line parameterization to 15 in CRG (1).

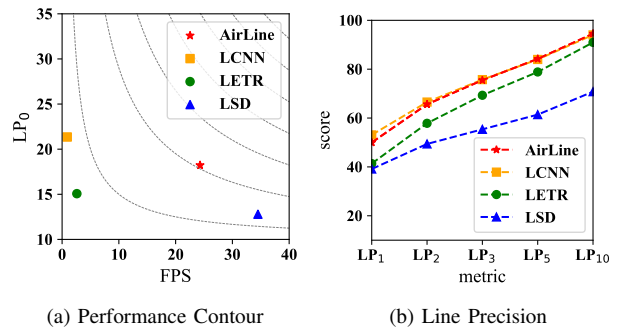


Fig. 7: Overall performance of AirLine. (a) is the performance contour (LP₀-FPS); The closer to the upper-right corner, the better the precision-speed performance. (b) presents line precision with different settings. LP₀ denotes different methods’ percentage probability to strictly cover GT pixels without dilation. Curves in (a) are defined by $y = \frac{LP_0 \cdot FPS}{x} + 10$, we offset y-coordinate by 10 because it can be taken as a baseline that can be produced by some random line detector.

B. Overall Performance

We first conduct a quantitative evaluation and compare with the state-of-the-art methods including LCNN [17], LETR [18], and LSD [12] using the widely-used Wireframe [21] dataset. It consists of a set of 5,000 images of housing structures, which is suitable for both training and accuracy tests. We present the LP scores and frames per second (FPS) on the test set in Table I, in which AirLine achieves comparable accuracy with the best-scored method LCNN but is of much higher runtime efficiency, i.e., roughly $25\times$ faster than LCNN. Some of the example outputs of different methods are shown in Fig. 8. For better visualization, we show the performance contour with LP₀ (the most strict metric) in Fig. 7a and the full LP scores in Fig. 7b. As can be seen, AirLine achieves the best overall performance in terms of balanced accuracy and efficiency with a large margin than other methods. It is noticeable that LSD achieves the 2nd best overall performance in Fig. 7a, which is also one of the reasons that LSD is still preferred nowadays over other more recent methods, e.g. LCNN, in robotic tasks.

C. Quantitative Generalization Test

We further test the generalization performance of AirLine by testing the model trained on Wireframe dataset on the YorkUrban [22] dataset. Different from Wireframe which primarily contains demonstration-level images, YorkUrban offers a larger variety of live shots across different environments, making it ideal for quantitative generalization tests. As shown in Table II and Fig. 9, although AirLine is the 2nd best in terms of accuracy but it still possesses the most notable balance between accuracy and speed, i.e., $80\times$ faster than LCNN. This exceptional speed and efficiency make AirLine a top-performing method for learnable real-time line detection, which is crucial for on-field robotics. Note that LSD achieves the 2nd best overall performance and ranks above LCNN and LETR in Fig. 9a, which further explains

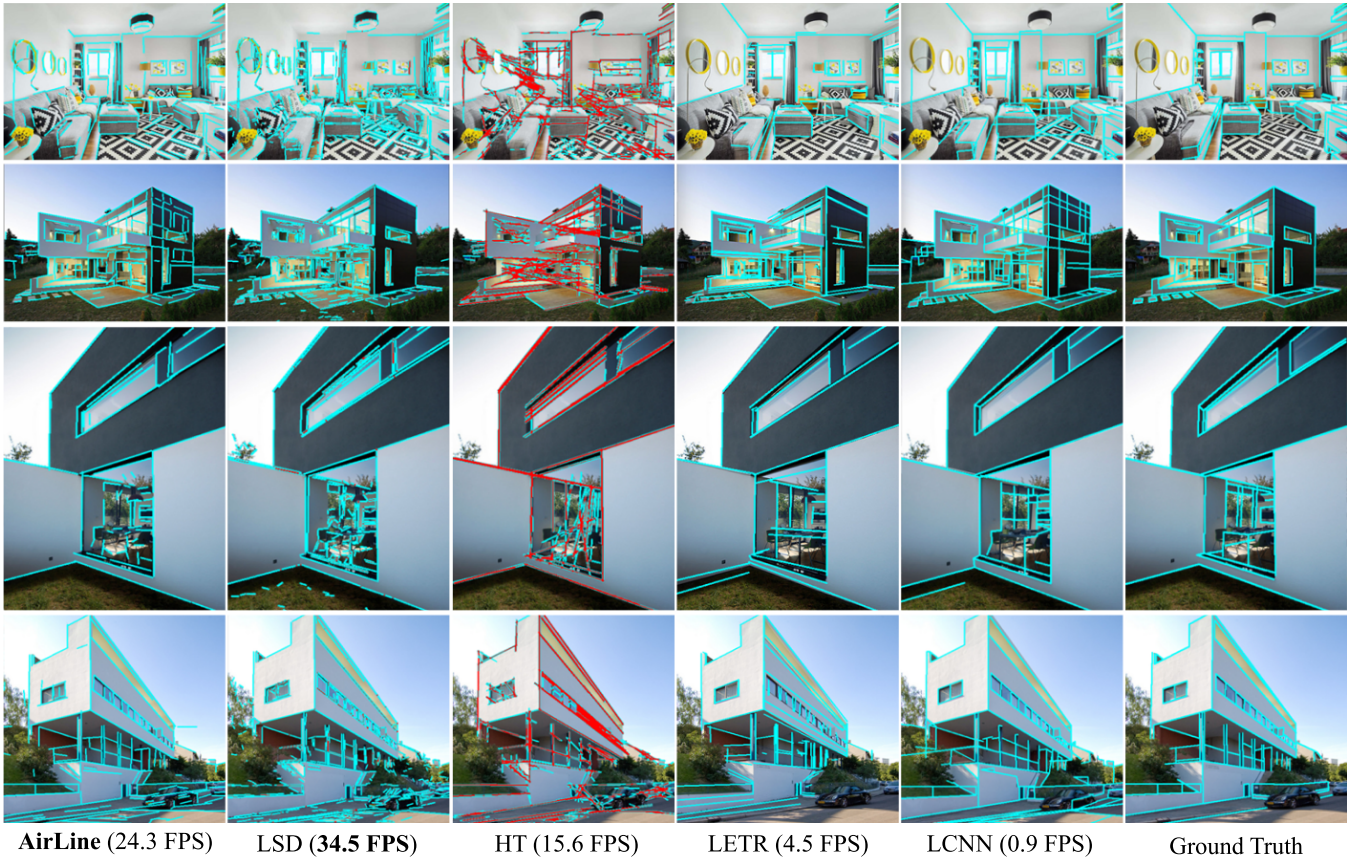


Fig. 8: The qualitative results on the Wireframe dataset [21]. Images to examine line quality, noisiness, and generalization ability of different methods on images from the test set. *HT contains overlapped lines and we use red color to highlight duplicate detection areas, while little line overlaps exist in other methods.

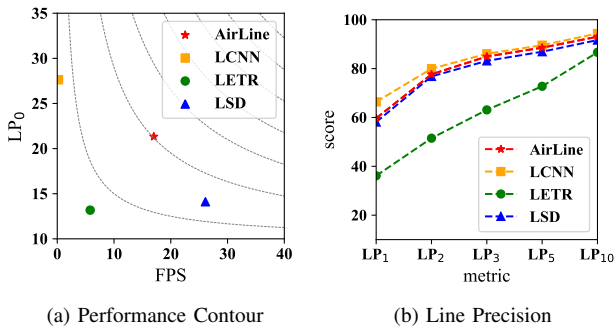


Fig. 9: Generalization Test. (a) and (b) are the performance counter and LP scores, respectively. In (b) the steepness of curves reflect the output stability: a less steep curve implies a more consistent score even given greater error. AirLine and LSD achieve the 1st and 2nd best generalization performance.

the popularity of LSD in robotic tasks and the rationality of the overall performance contour compared to sole accuracy.

D. Qualitative Generalization Test

We next present the qualitative generalization test using online images and the UMA-VI [30] dataset. UWA-VI doesn't offer ground truth lines for evaluation but it is ideal

TABLE II: Generalization test.

Method	LP ₀	LP ₁	LP ₂	LP ₃	LP ₅	LP ₁₀	FPS
AirLine	<u>21.33</u>	<u>59.66</u>	<u>77.66</u>	<u>84.95</u>	<u>88.58</u>	<u>93.06</u>	<u>17.0</u>
LCNN	27.63	66.39	79.96	86.08	89.59	94.37	0.21
LETR	13.18	36.14	51.52	63.10	72.76	86.66	5.8
LSD	14.11	58.12	76.80	83.17	86.91	91.68	26.1

for generalization tests especially for robotic applications, since it provides low-textured subterranean environments and scenes with dynamic illumination, which was adopted in the well-known DARPA SubT challenge [31], [32]. As shown in Fig. 10, we found that the AirLine and LSD methods performed better than the LETR and LCNN in generating detailed line detections. Moreover, AirLine is preferred over LSD since it is able to merge the two sides of thin lines, while LSD tends to detect both sides. Though LCNN produces lines of high precision, it is not suitable for tasks that require detailed line inputs, as it tends to ignore short lines and connect two unrelated endpoints in complex environments. LETR, which performed the best under the endpoint precision mentioned in its original paper, was found to have the worst line quality in terms of precision, stability, and reasonable geometry. In addition, we test the Hough

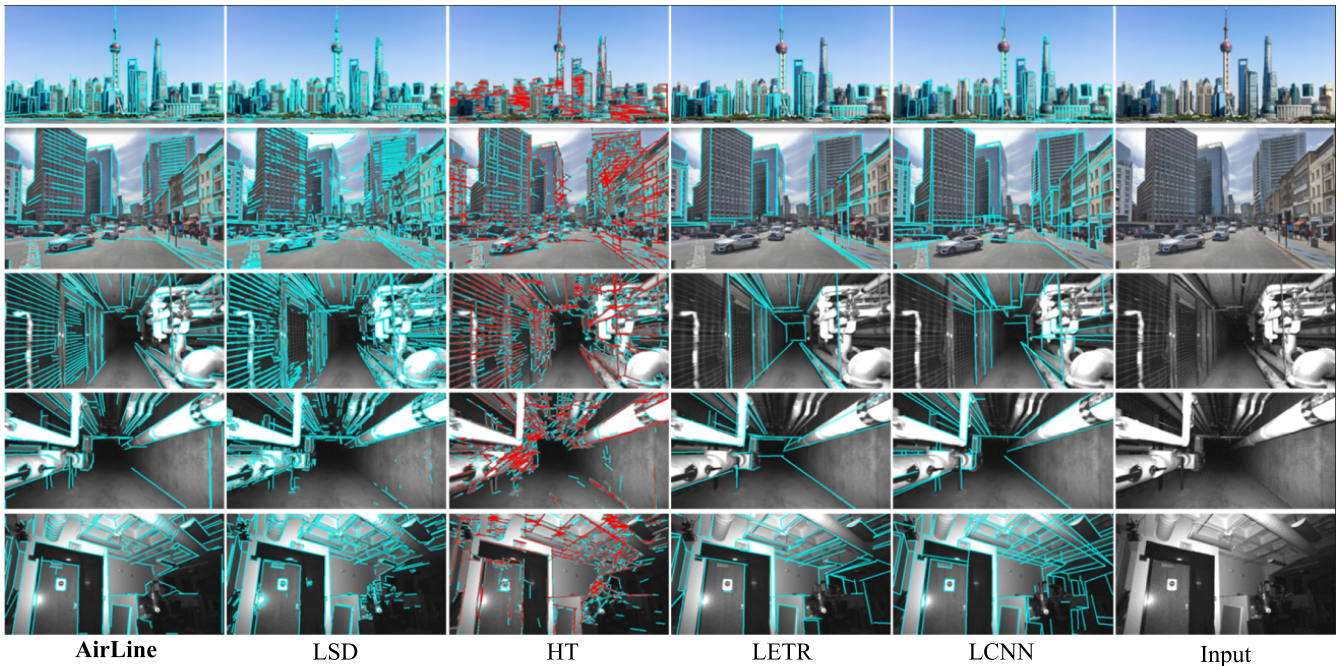


Fig. 10: Generalization test on online images and monochrome sequences of subterranean environments. We also highlighted overlap detection in red as done in Fig. 8. The first row is a distant view of city and the second row is street view, while the third to fifth rows are from UMA-VI [30].

TABLE III: Ablation study of orientation descriptor.

CRG input	LP ₀	LP ₁	LP ₂	LP ₃	LP ₅	LP ₁₀
6-channel OD	21.33	59.66	77.66	84.95	88.58	93.06
2-channel OD	16.95	46.59	62.14	71.91	80.28	90.72
Image gradient	13.70	37.43	50.11	58.86	67.48	80.15

Transform [13] (implemented by OpenCV) in conjunction with our edge detector as a baseline of edge-to-line methods. It produces a large number of overlapping lines, while AirLine and others have almost no overlapped detection.

E. Ablation Study

In addition, we conducted an ablation study on the orientation descriptor, a critical component of AirLine that connects learnable modules with handcraft algorithms. As presented in Table III, we tested and compared three different orientation detection (OD) as input for conditional region grow: 6-channel orientation descriptor as proposed in Section III-B; 2-channel orientation descriptor, using only 0° and 90° kernels shown in Fig. 3; and 2-channel image gradient. By comparing the LP scores produced by 6-channel OD and 2-channel OD, we can see that the 6 channels perform better, though 2 channels are theoretically sufficient to describe the horizontal and vertical edges. By comparing the 2-channel orientation descriptor to 2-channel image gradient, we can see that our orientation descriptor can support more precise pixel-level detection (higher LP₀ score) and better semantic awareness (higher LP₁₀ score, which means that detector can cover more lines given greater tolerance). Therefore, our

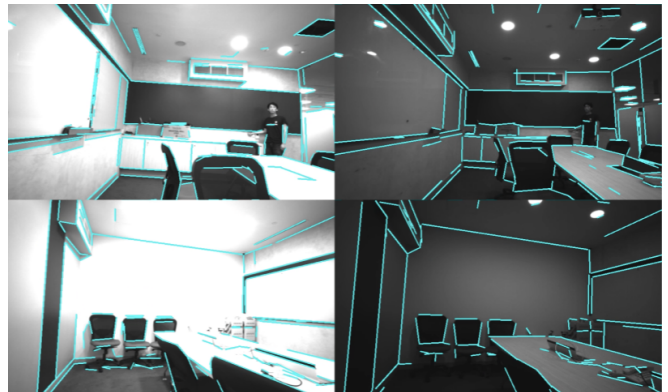


Fig. 11: A live demo shot in an office environment. Airline succeeded at producing a stable consistent detection with significant illumination changes.

orientation detector is crucial for accurate edge segmentation, and the ablation study confirms its effectiveness.

F. Live Demo

We further present a live demo and show four snapshots in Fig. 11 to demonstrate the robustness of AirLine. The goal is to detect lines as consistently as possible given changing illumination and viewport. We observed a stable line detection even though the brightness in the environment is changing frequently: The left two images present two over-exposure frames while the right presents much darker frames of the same scene. Existing methods could be largely interfered by the illumination change and produce inconsistent line

detection at the same place, while AirLine kept track of most significant lines from the over-exposed frame to the other frames. For better visualization, we suggest the readers watch the video attached to this paper.

V. CONCLUSION

We present AirLine, a novel line segment detection method, and demonstrated that it can effectively generalize to various scenes without a significant increase in processing time compared to the state-of-the-art methods. Specifically, we introduce a new scheme for edge-to-line detection, which overcomes the instability of point-to-line methods and the low efficiency of other learnable methods. We also propose a new line segment detection metric that emphasizes pixel-level accuracy, which is more demanded in many robotic tasks like SLAM. AirLine achieves state-of-the-art-level precision with a significant 3 – 80× runtime acceleration. Our comparisons and a live demo show that AirLine is effective for real-world scenarios and robust to environmental changes.

REFERENCES

- [1] C. Wang, W. Wang, Y. Qiu, Y. Hu, and S. Scherer, "Visual Memorability for Robotic Interestingness via Unsupervised Online Learning," in *European Conference on Computer Vision*, vol. 12347 LNCS, 2020.
- [2] Y. Qiu, C. Wang, W. Wang, M. Henein, and S. Scherer, "Airdos: dynamic slam benefits from articulated objects," in *International Conference on Robotics and Automation (ICRA)*, 2022, pp. 8047–8053.
- [3] H. Caesar, V. Bankiti, A. H. Lang, S. Vora, V. E. Liong, Q. Xu, A. Krishnan, Y. Pan, G. Baldan, and O. Beijbom, "Nuscenes: A multimodal dataset for autonomous driving," in *Proceedings of the IEEE Computer Society Conference on Computer Vision and Pattern Recognition*, 2020.
- [4] V. Kolmogorov and R. Zabih, "Multi-camera scene reconstruction via graph cuts," in *Lecture Notes in Computer Science (including subseries Lecture Notes in Artificial Intelligence and Lecture Notes in Bioinformatics)*, vol. 2352, 2002.
- [5] P. E. Sarlin, D. Detone, T. Malisiewicz, and A. Rabinovich, "SuperGlue: Learning Feature Matching with Graph Neural Networks," in *Proceedings of the IEEE Computer Society Conference on Computer Vision and Pattern Recognition*, 2020.
- [6] D. Detone, T. Malisiewicz, and A. Rabinovich, "SuperPoint: Self-supervised interest point detection and description," in *IEEE Computer Society Conference on Computer Vision and Pattern Recognition Workshops*, vol. 2018-June, 2018.
- [7] A. Vakhtov and V. Lempitsky, "Learnable Line Segment Descriptor for Visual SLAM," *IEEE Access*, vol. 7, 2019.
- [8] V. N. Nguyen, R. Jenssen, and D. Roverso, "LS-Net: fast single-shot line-segment detector," *Machine Vision and Applications*, vol. 32, no. 1, 2021.
- [9] J. Ma, X. Jiang, A. Fan, J. Jiang, and J. Yan, "Image Matching from Handcrafted to Deep Features: A Survey," *International Journal of Computer Vision*, vol. 129, no. 1, 2021.
- [10] S. Brahmabhatt, J. Gu, K. Kim, J. Hays, and J. Kautz, "Geometry-Aware Learning of Maps for Camera Localization," in *Proceedings of the IEEE Computer Society Conference on Computer Vision and Pattern Recognition*, 2018.
- [11] F. Amigoni and V. Caglioti, "An information-based exploration strategy for environment mapping with mobile robots," *Robotics and Autonomous Systems*, vol. 58, no. 5, 2010.
- [12] R. Grompone Von Gioi, J. Jakubowicz, J. M. Morel, and G. Randall, "LSD: A fast line segment detector with a false detection control," *IEEE Transactions on Pattern Analysis and Machine Intelligence*, vol. 32, no. 4, 2010.
- [13] R. O. Duda and P. E. Hart, "Use of the Hough Transformation to Detect Lines and Curves in Pictures," *Communications of the ACM*, vol. 15, no. 1, 1972.
- [14] J. Canny, "A Computational Approach to Edge Detection," *IEEE Transactions on Pattern Analysis and Machine Intelligence*, vol. PAMI-8, no. 6, 1986.
- [15] Q. Yu, G. Xu, Y. Cheng, and Z. H. Zhu, "PLSD: A Perceptually Accurate Line Segment Detection Approach," *IEEE Access*, vol. 8, 2020.
- [16] C. Wang, D. Gao, K. Xu, J. Geng, Y. Hu, Y. Qiu, B. Li, F. Yang, B. Moon, A. Pandey, Aryan, J. Xu, T. Wu, H. He, D. Huang, Z. Ren, S. Zhao, T. Fu, P. Reddy, X. Lin, W. Wang, J. Shi, R. Talak, K. Cao, Y. Du, H. Wang, H. Yu, S. Wang, S. Chen, A. Kashyap, R. Bandaru, K. Dantu, J. Wu, L. Xie, L. Carlone, M. Hutter, and S. Scherer, "PyPose: A library for robot learning with physics-based optimization," in *IEEE/CVF Conference on Computer Vision and Pattern Recognition (CVPR)*, 2023.
- [17] Y. Zhou, H. Qi, and Y. Ma, "End-to-end wireframe parsing," in *Proceedings of the IEEE International Conference on Computer Vision*, vol. 2019-October, 2019.
- [18] Y. Xu, W. Xu, D. Cheung, and Z. Tu, "Line Segment Detection Using Transformers without Edges," in *Proceedings of the IEEE Computer Society Conference on Computer Vision and Pattern Recognition*, 2021.
- [19] K. Zhao, Q. Han, C. B. Zhang, J. Xu, and M. M. Cheng, "Deep Hough Transform for Semantic Line Detection," *IEEE Transactions on Pattern Analysis and Machine Intelligence*, vol. 44, no. 9, 2022.
- [20] N. G. Cho, A. Yuille, and S. W. Lee, "A Novel Linelet-Based Representation for Line Segment Detection," *IEEE Transactions on Pattern Analysis and Machine Intelligence*, vol. 40, no. 5, 2018.
- [21] K. Huang, Y. Wang, Z. Zhou, T. Ding, S. Gao, and Y. Ma, "Learning to Parse Wireframes in Images of Man-Made Environments," in *Proceedings of the IEEE Computer Society Conference on Computer Vision and Pattern Recognition*, 2018.
- [22] P. Denis, J. H. Elder, and F. J. Estrada, "Efficient edge-based methods for estimating manhattan frames in urban imagery," in *Lecture Notes in Computer Science (including subseries Lecture Notes in Artificial Intelligence and Lecture Notes in Bioinformatics)*, vol. 5303 LNCS, no. PART 2, 2008.
- [23] N. Xue, T. Wu, S. Bai, F. Wang, G. S. Xia, L. Zhang, and P. H. Torr, "Holistically-Attracted Wireframe Parsing," in *Proceedings of the IEEE Computer Society Conference on Computer Vision and Pattern Recognition*, 2020.
- [24] N. Carion, F. Massa, G. Synnaeve, N. Usunier, A. Kirillov, and S. Zagoruyko, "End-to-End Object Detection with Transformers," in *Lecture Notes in Computer Science (including subseries Lecture Notes in Artificial Intelligence and Lecture Notes in Bioinformatics)*, vol. 12346 LNCS, 2020.
- [25] E. S. Lev Teplyakov, Leonid Erlygin, "Lsdnet: Trainable modification of lsd algorithm for real-time line segment detection," in *IEEE Access*, 2022, pp. 45 256–65.
- [26] O. Ronneberger, P. Fischer, and T. Brox, "U-net: Convolutional networks for biomedical image segmentation," in *Lecture Notes in Computer Science (including subseries Lecture Notes in Artificial Intelligence and Lecture Notes in Bioinformatics)*, vol. 9351, 2015.
- [27] A. Paszke, S. Gross, F. Massa, A. Lerer, J. Bradbury, G. Chanan, T. Killeen, Z. Lin, N. Gimelshein, L. Antiga, A. Desmaison, A. Köpf, E. Yang, Z. DeVito, M. Raison, A. Tejani, S. Chilamkurthy, B. Steiner, L. Fang, J. Bai, and S. Chintala, "PyTorch: An imperative style, high-performance deep learning library," in *Advances in Neural Information Processing Systems*, vol. 32, 2019.
- [28] D. P. Kingma and J. L. Ba, "Adam: A method for stochastic optimization," in *3rd International Conference on Learning Representations, ICLR 2015 - Conference Track Proceedings*, 2015.
- [29] G. Bradski, "The OpenCV Library," *Dr. Dobb's Journal of Software Tools*, 2000.
- [30] David Zuñiga-Noël, Alberto Jaenal, Ruben Gomez-Ojeda, and Javier Gonzalez-Jimenez, "The UMA-VI dataset: Visual-inertial odometry in low-textured and dynamic illumination environments," *SAGE Journals*, 7 2020.
- [31] S. Scherer, V. Agrawal, G. Best, C. Cao, K. Cujic, R. Darnley, R. DeBortoli, E. Dexheimer, B. Drozd, R. Garg, *et al.*, "Resilient and modular subterranean exploration with a team of roving and flying robots," *Field Robotics Journal*, pp. 678–734, May 2022.
- [32] K. Ebadi, L. Bernreiter, H. Biggie, G. Catt, Y. Chang, A. Chatterjee, C. E. Denniston, S.-P. Deschênes, K. Harlow, S. Khattak, *et al.*, "Present and future of slam in extreme underground environments," *arXiv preprint arXiv:2208.01787*, 2022.